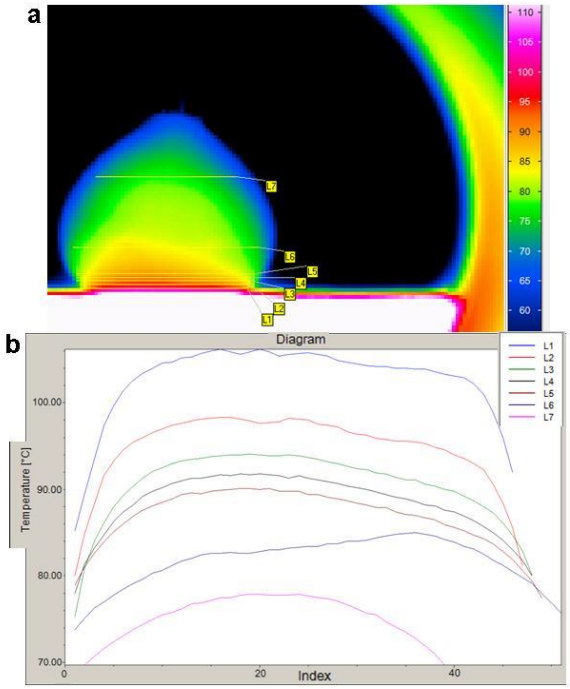

Supplementary Figure S1

IR-Temperature measurement inside a levitated droplet: a, The cross sectional thermograph view of the levitated drop (~ 400 µL) on aluminum substrate at 250 °C shows different colors which related to different temperatures. For these measurements, the edge of substrate (which facing toward the camera) were coated with a varnish spray to increase their emissivity (Tetenal camera varnish, emissivity 0.96). There are seven horizontal lines at different levels through the drop, which show the temperature of the different area of drop during levitation where the temperature inside the drop decreases from down to up. **b,** The graph, which calculated automatically by the software of the camera, shows the temperature gradient corresponding to each line drown in part a. It clearly demonstrate the temperature variation inside and at the edge of the drop.

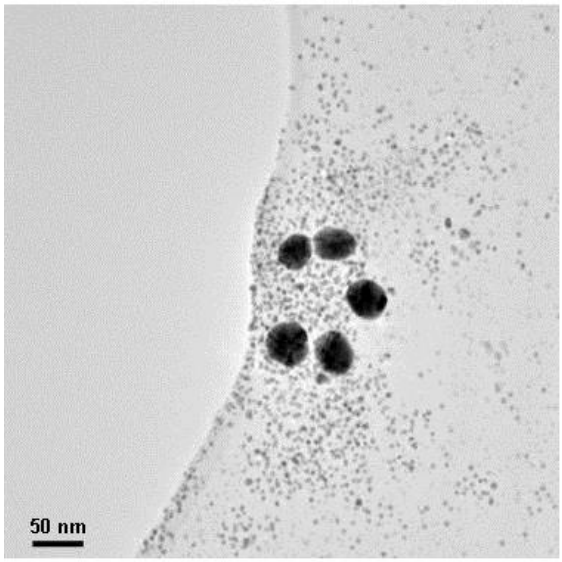

Supplementary Figure S2
TEM image of bigger gold nanoparticles: Bright field TEM image of few ~40 nm gold particles which might be formed due to further growth at the air liquid interface or during drying on the TEM Grid.

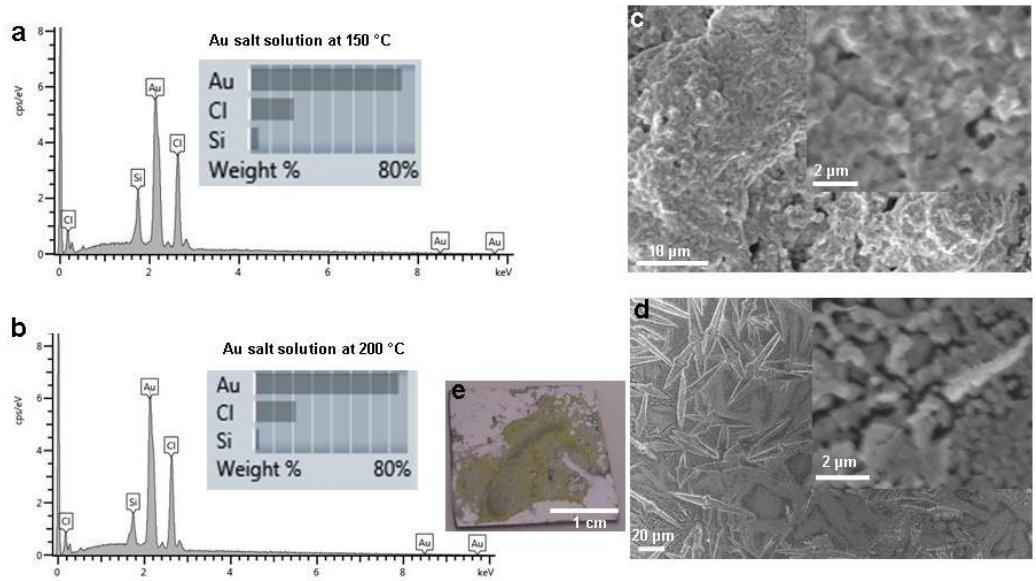

Supplementary Figure S3
Characterization of gold chloride solution heated at lower temperature than the Leidenfrost: a, EDX spectra of 50 µL droplet of 20 mM solution placed on silicon substrate heated at 150 ˚C. **b,** at 200 ˚C. Inset in each graph shows the chemical composition in percentage. **c & d,** SEM images of samples (a) and (b) with 2 magnification, correspondingly. **e**, The photograph of the analyzed sample at 200°C.

Supplementary Figure S4
Detection of chlorine gas in the vapor: Syringaldazine was placed on a glass substrate and the glass substrate was set above a Leidenfrost drop of $AuCl_4^-$ solution. A change in the color of syringaldazine from colorless to red-purple indicates a reaction with chlorine in the vapor.

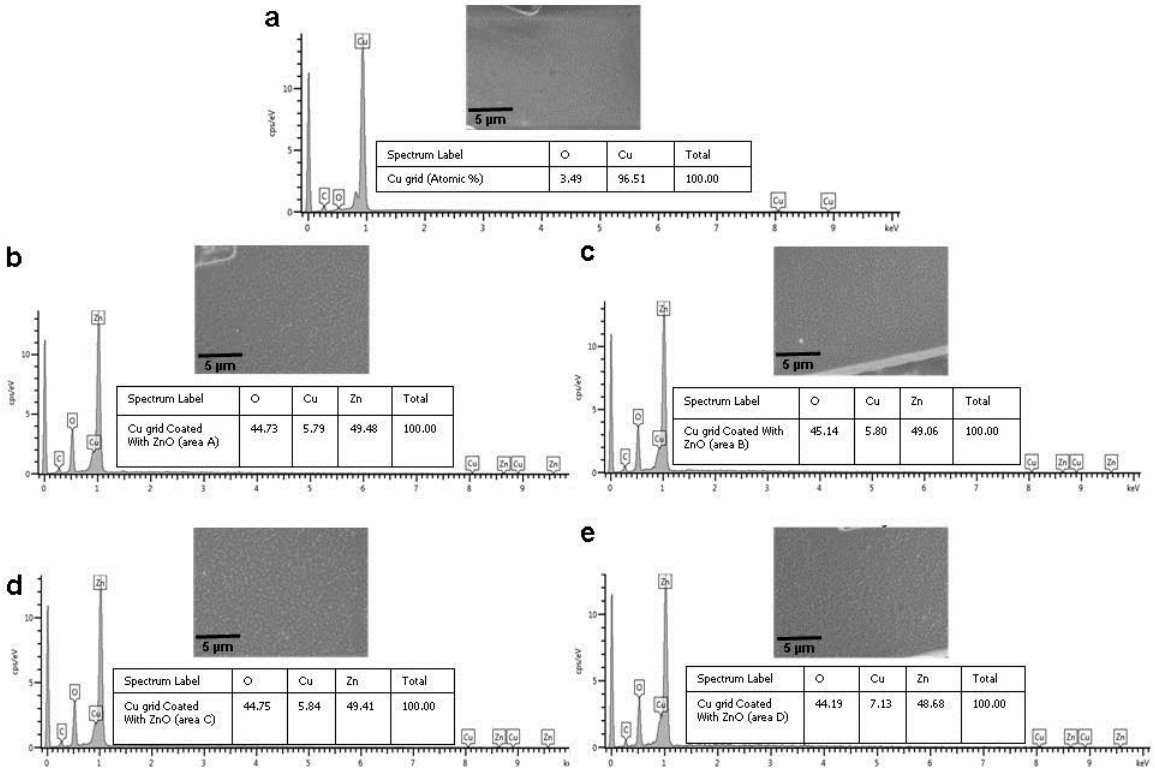

Supplementary Figure S5
EDX analysis of ZnO coating on the TEM grid: a, uncoated Cu grid. **b, c, d & e** coated with ZnO, at four different regions. Insets in each graph represents the corresponding SEM image and chemical composition (atomic %) of each area.

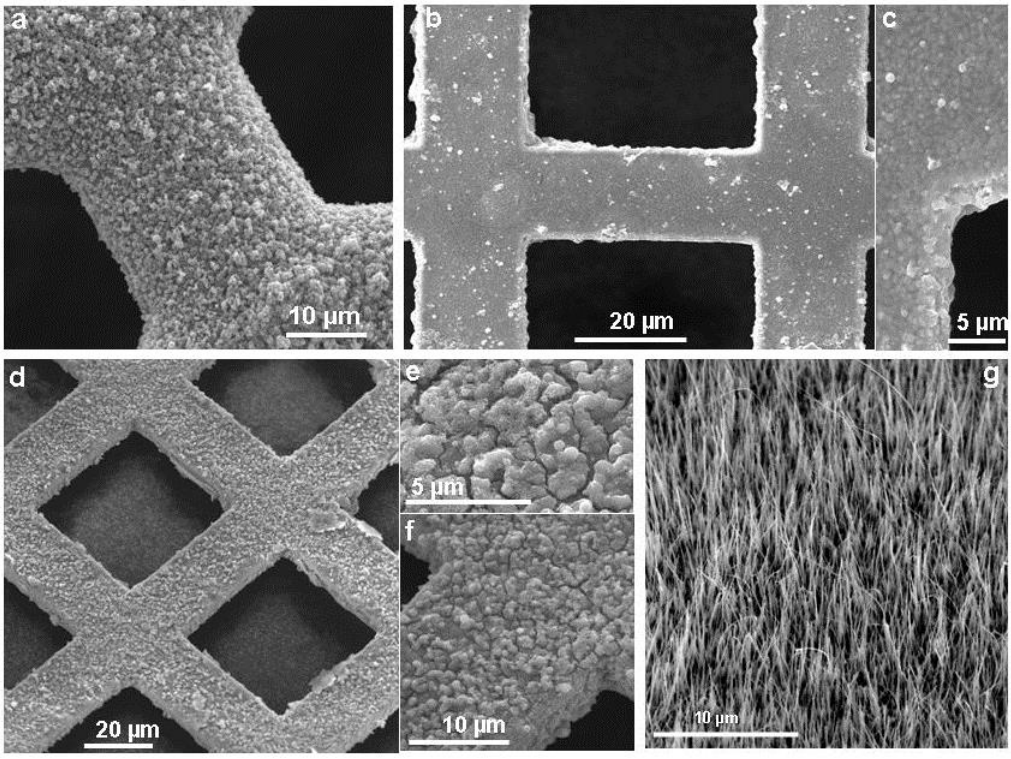

Supplementary Figure S6

SEM images of ZnO and CuO coating on the TEM grid: a, a thicker coating by using 40 mM zinc acetate aqueous solution. **b & c,** with 2 times coating by using 20 mM zinc acetate at low and high magnification, respectively. **d, e & f,** with 5 times coated sample at low and higher magnification. **g,** The nanograss (CuO) with few micrometer length and few tens of nanometers diameter which covers the surface due to further heat treatment for 2 hours at 400°C.

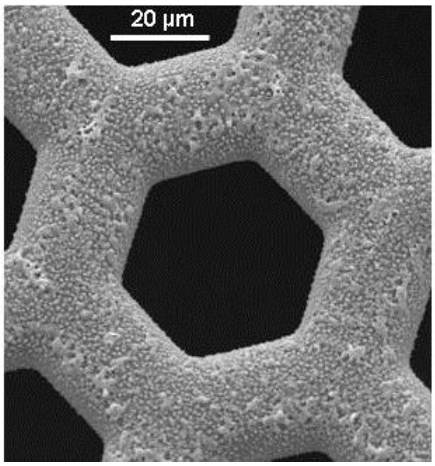

Supplementary Figure S7
Inhomogeneous ZnO coating: ZnO film coated at the same conditions as of Fig. 3b. The non-uniformity of the film is apparent which might have originated from the bubble formation during the process.

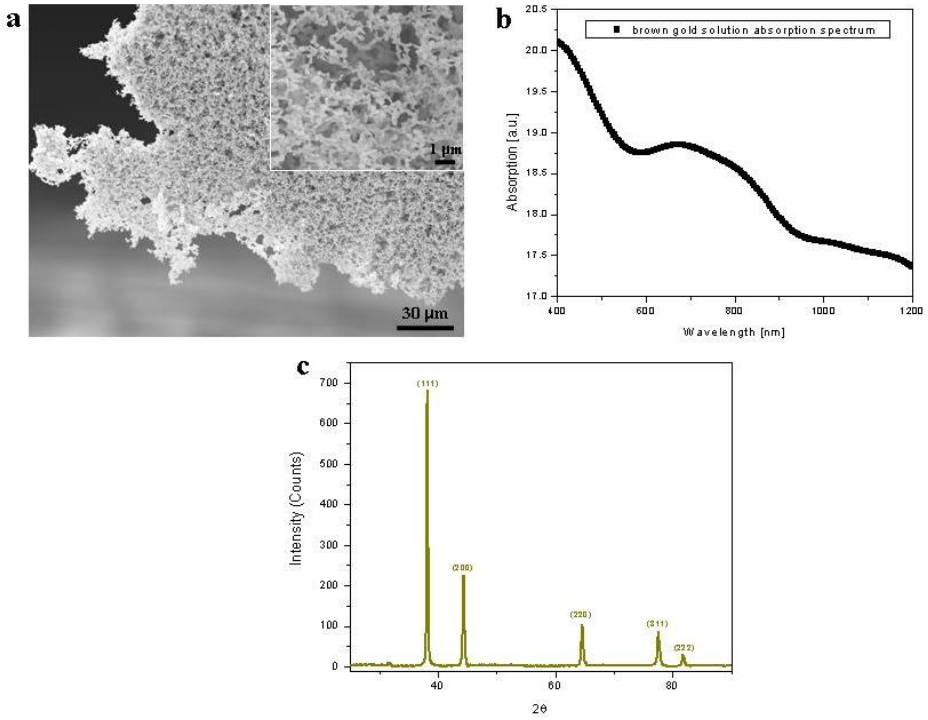

Supplementary Figure S8
SEM, absorption spectra and XRD pattern of brown spongy gold: a, scanning electron microscopy image of structure of brown spongy gold. **b,** UV/Vis absorption spectra of brown spongy gold suspension (Fig. 4c) in visible and NIR wavelength. **c,** XRD pattern of brown spongy gold. Diffraction peaks at 2θ = 38.2°, 44.4°, 64.6°, 77.6° and 81.7° corresponds to (111), (200), (220), (311) and (222) planes of pure Gold.

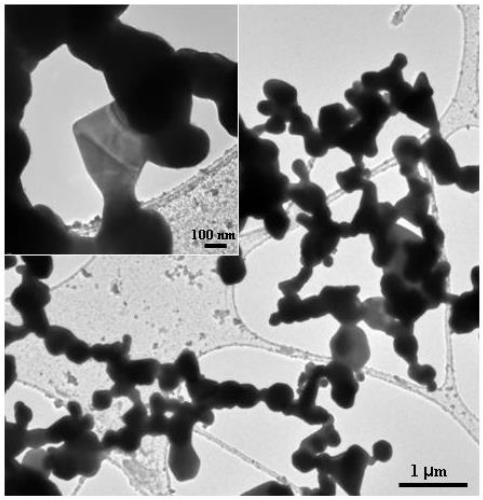

Supplementary Figure S9
TEM analysis of spongy gold produced by gold salt with sod. citrate only: TEM image of spongy gold showing a porous network formed through fusion of particles by particle impingement and coalescence to some extent.

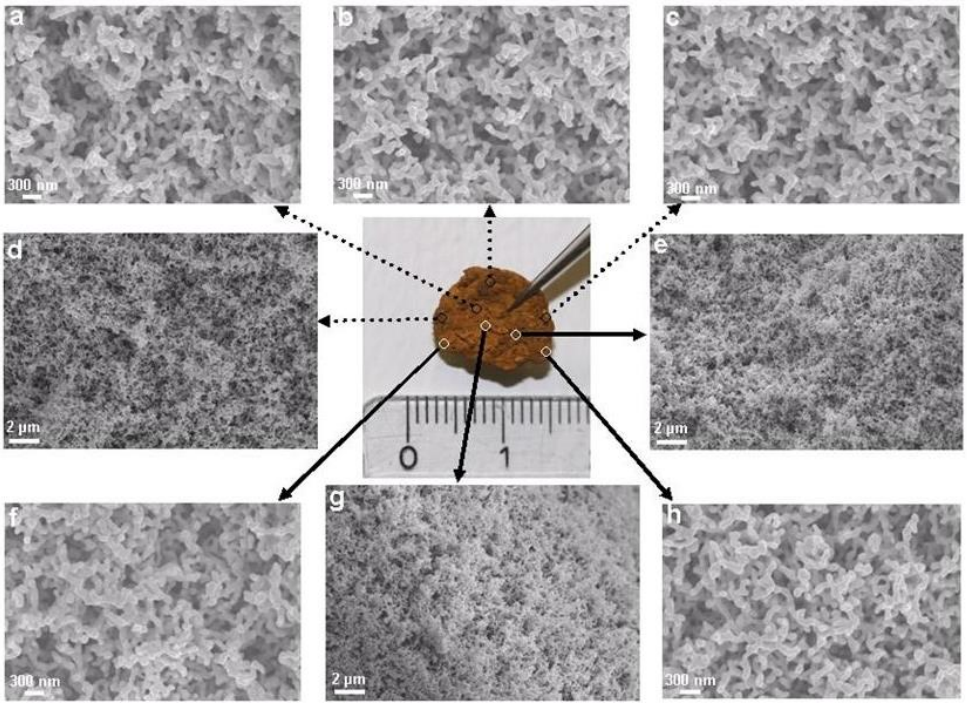

Supplementary Figure S10
Investigation of the uniformity of the sponge nanoporous gold sample shown in Fig. 4i: a, b, c & d, SEM images of the top surface at different places shows the uniformity for the porous structure. **e, f, g & h,** the backside at different points. The photograph of the analyzed sample is also shown for clarity.

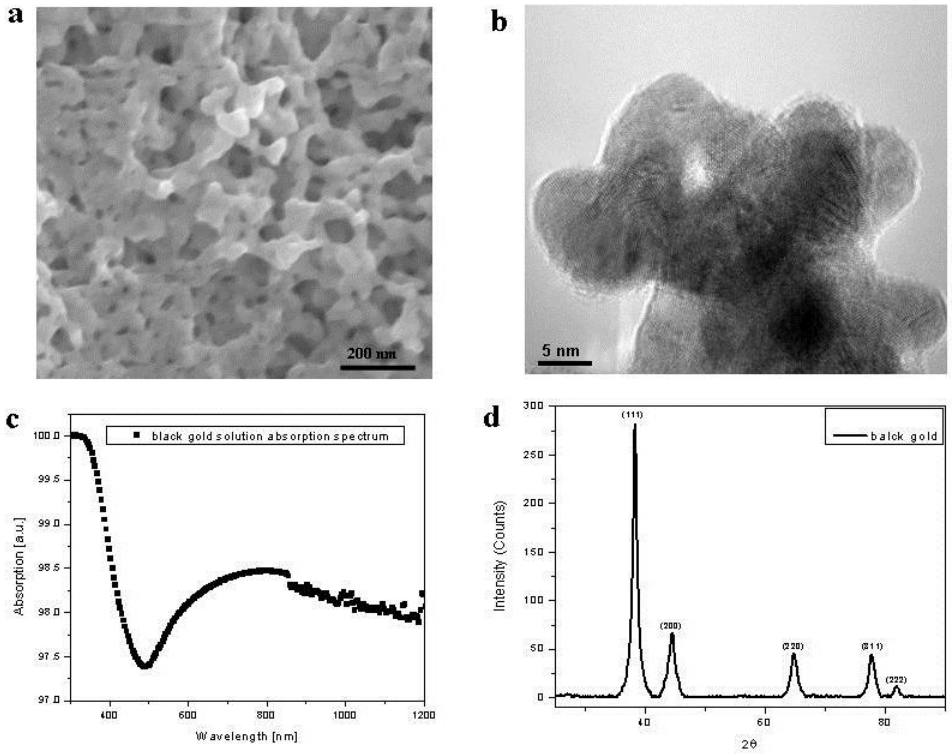

Supplementary Figure S11

SEM, TEM, absorption spectra and XRD pattern of black spongy gold : a, scanning **b,** high resolution TEM (HRTEM) images confirms the presence of pure Au and reveals that the nanoparticles have tightly merged together to form interconnected structures.

c, absorption spectra of black spongy gold in visible and NIR wavelength. **d,** XRD pattern of black spongy gold. Diffraction peaks at $2\theta = 38.2°$, $44.4°$, $64.6°$, $77.6°$ and $81.7°$ corresponds to (111), (200), (220), (311) and (222) planes of pure Gold.

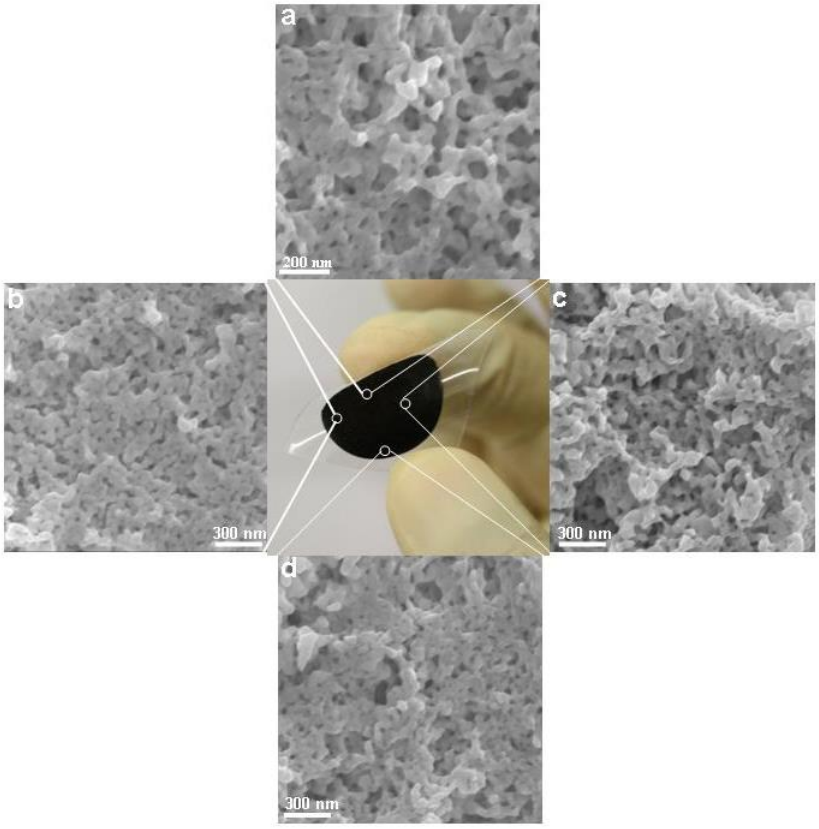

Supplementary Figure S12
Investigation of the uniformity of the black nanoporous gold sample shown in Fig. 5a: a, b, c & d, SEM images of porous film on flexible polymeric substrate at different area show the uniformity of the porous structure of the sample. The photograph of the characterized sample is shown in the middle.

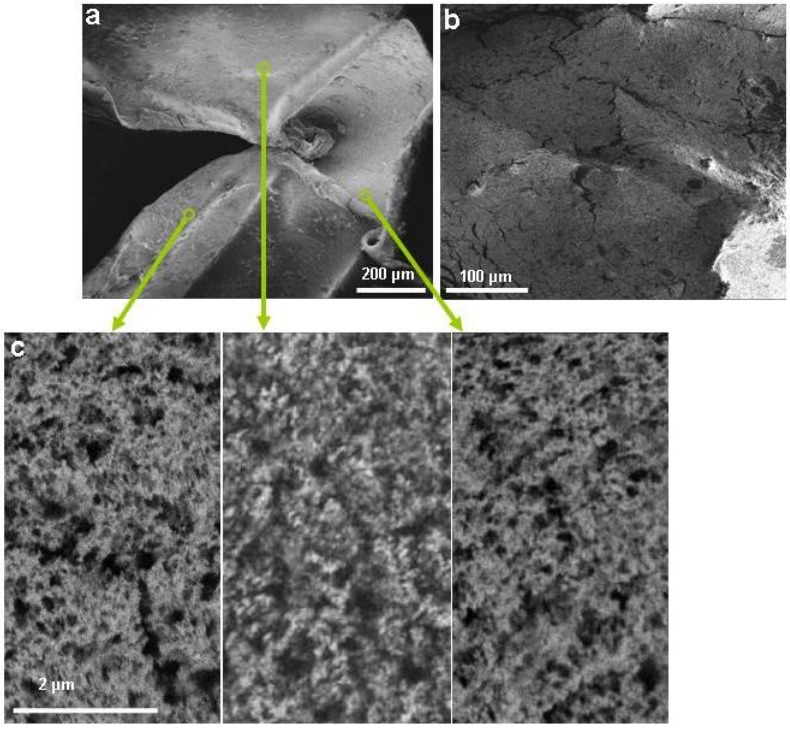

Supplementary Figure S13
SEM images, of polymer foam coated with black gold, at 3 different magnifications: **a,** low. **b,** moderate. **c,** high magnification of 3 different areas, respectively.

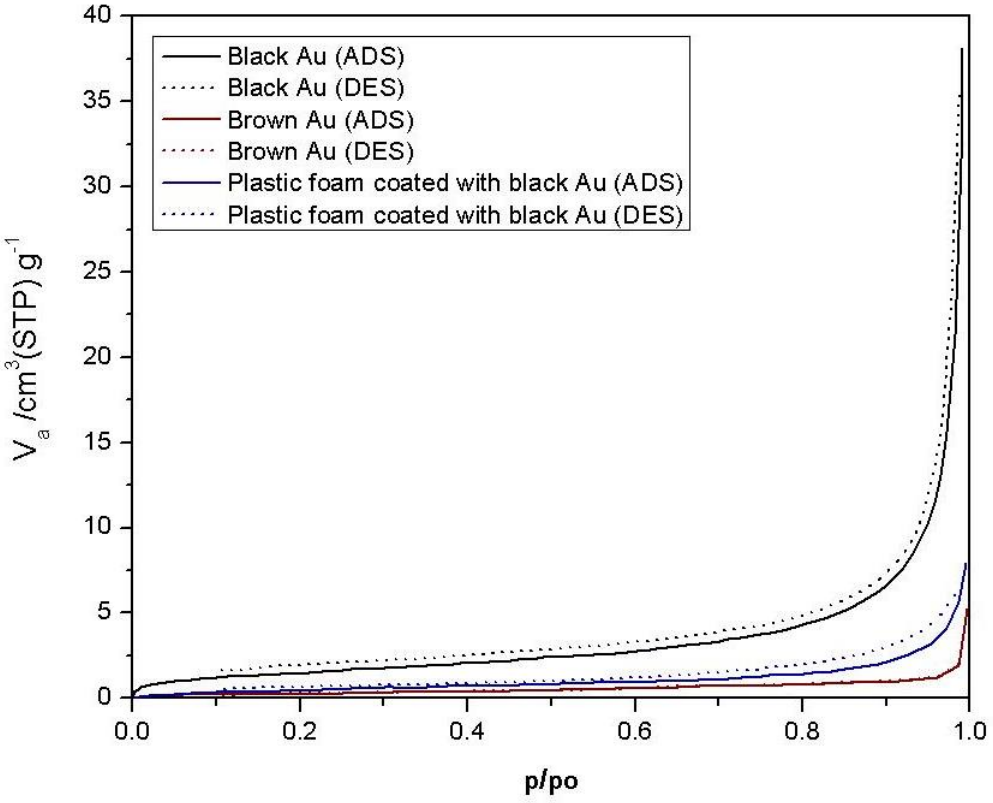

Supplementary Figure S14
BET analysis : Nitrogen adsorption (ADS)\desorption (DES) curves of the spongy brown, black and hybrid foam gold samples activated at room temperature over night under vacuum at the same parameters.

Supplementary Table S1

BET analysis of spongy brown, black and hybrid gold samples

Parameters [unit]	**Brown Au**	**Black Au**	**Polymer / black Au**
$\mathbf{V_m}$ [cm^3(STP) g^{-1}]	0.2218	1.2985	0.4713
$\mathbf{a_{s,BET}}$ [m^2 g^{-1}]	0.96518	5.6516	2.0513
C	155.31	50.667	17.94
Total pore volume (p/p_0=0.500) [cm^3 g^{-1}]	0.000752	0.003785	0.0012507
Average pore diameter [nm]	3.1175	2.6786	2.4388

where (V_m**)** is monolayer adsorbed gas quantity, ($a_{s,BET}$) is specific surface area and (c**)** is BET constant.

Supplementary Note 1

Mechanism of gold reduction

The suggested chemical pathway for the formation of gold nanoparticles follows a multistep reduction mechanism of Au (III) ions into elemental Au through an intermediate state Au(I) ions (i.e. Dichloroaurate) with the release of chlorine/free chlorine gas. This process is facilitated by the Hydroxide ions which promote both basic conditions and electron transfer reactions[29,30]. Thus, the postulated overall reaction can be written as follows:

$$2\ OH^- + AuCl_4^- = \tfrac{1}{2}O_2 + H_2O + Au^o + 2\ Cl_2 \qquad (S1)$$

Chlorine gas was indicated by using a FACTS method[48,49]. This method is based on the reaction of colorless 3,5-dimethyl-4-hydroxybenzaldazine (syringaldazine) with chlorine /free chlorine (i.e. can be formed if chlorine gas is dissolved in hot water under basic condition) leading to the formation of a red-purple azo-compound. The condensed vapor of the levitated drop was used to prevent any effect from the chloride ions of the salt inside the drop. A positive result was directly registered at the early stage of levitation as shown in Supplementary Fig. S4 (before the plasmonic color change in the drop was observed). Indeed oxidation of chlorine ions to chlorine gas as indicated in the vapor implies the presence of Au(I) (i.e. $AuCl_2^-$) as a transient in the levitated droplet.

Au (I) ions formed as intermediate are reduced to neutral gold atom either by accepting electrons from the OH^- ions or due to the following disproportionation reaction[50]:

$$3\ AuCl_2^- = AuCl_4^- + 2\ Au^o + 2\ Cl^- \qquad (S2)$$

The reaction is generally occurred under basic condition which is fulfilled in the Leidenfrost droplet as proved by us.

As recently shown[51], the association of gold atoms with excess of Au(I) ions is followed by their coalescence into gold clusters, where the further reduction of Au(I) ions

is catalyzed by the formed gold nanoclusters in organic solvents (e.g. Alcohols). We expect that this process occurs under the Leidenfrost conditions as water at a temperature between 100 and 200°C behaves like an organic solvent (i.e. water-methanol mixture)[52] owing to the disruption of the hydrogen bond network at the hot interface. Additionally this process is even accelerated and enhanced by the local accumulation of the ions and the increase of diffusion rate owing to the fast phase expansion and global evaporation of the Leidenfrost droplet and thus satisfying a vital condition for the nucleation and growth of the gold clusters.

Finally, it is worth mentioning here that, a titration test with different molarities and volumes, of NaOH solution did not show any trace of HCl neither in the vapor nor in the droplet which agrees well with our suggested reaction pathway.

Supplementary Note 2

Coating inside Leidenfrost droplet

Thicker coating achieved by increasing the concentration (Supplementary Fig. S6a), was also done by multiple steps coating. Two samples were prepared by coating TEM grids with ZnO in multiple steps. SEM images, (Supplementary Fig. S6b, c), of double coated grid show minor defects in the form of "cluster agglomeration" on the surface of the film. This effect became even worse in case of 5 times deposition, as shown in (Supplementary Fig. S6d). Higher magnified images (Supplementary Fig. S6e,f) further showed that, cracks had also been initiated on the film which ruined its quality. It seems that coating of the pre-coated sample does not produce a homogeneous film and the smoothness and uniformity would be sacrificed at the expense of thickness.

Supplementary References

48. Liebermann, J., Roscher, N. M., Meier, E. P. & Cooper, W. J. Development of the FACTS Procedure for Combined Forms of Chlorine and Ozone in Aqueous Solutions. *Environ. Sci. Technol.* **14(11),** 1395-1400 (1980).
49. Chriswell, B. & O'Halloran, K. R. Acid Yellow 17 as a spectrophotometric reagent for the determination of low concentrations of residual free chlorine. *Anal. Chim. Acta* **249(2)**, 519-524 (1991).
50. Au, L., Lu, X. & Xia, Y. A Comparative Study of Galvanic Replacement Reactions Involving Ag Nanocubes and $AuCl2^{-}$ or $AuCl4^{-}$. *Adv. Mater.* **20**, 2517-2522 (2008).
51. Dey, G. R., El Omar, A. K., Jacob, J. A., Mostafavi, M. & Belloni, J. Mechanism of Trivalent Gold Reduction and Reactivity of Transient Divalent and Monovalent Gold Ions Studied by Gamma and Pulse Radiolysis. *J. Phys. Chem. A* **115**, 383-391 (2011).
52. Clifford, A. A. Separations Using Superheated Water, Green Separation Processes. Wiley-VCH Verlag GmbH & Co. KGaA**:** 323-339 (2006).